CERN-SPSC-2006-018
SPSC-SR-009
29.06.2006

Status Report of the CAST Experiment

The CAST Collaboration

CEA-Saclay – CERN – Dogus University – Hellenic Open University Patras – Lawrence Livermore National Laboratory – Max-Planck-Institut für extraterrestrische Physik – Max-Planck-Institut für Physik – National Center for Scientific Research Demokritos – Rudjer Boskovic Institute – Institute for Nuclear Research (Moscow) – TU Darmstadt – University of British Columbia – University of Chicago – Universität Frankfurt – Universität Freiburg – University of Florida – University of Patras – University of South Carolina – University of Thessaloniki – Universidad de Zaragoza

1 Introduction

This report describes the scientific status of the CAST experiment, focussing on the work performed since the last SPSC meeting. Three main guidelines have led the work of the CAST collaboration during the last year:

- The upgrade of the experimental setup to operate the second phase of the experiment, namely the insertion of a buffer gas inside the magnet pipes, with accurately adjustable density, to recover the coherence of the axion-photon conversion for higher axion masses, and extend accordingly the sensitivity of CAST to axion masses above 0.02 eV.
- The commission the experiment in its new setup, and start the new phase of physics runs. Start exploring the analysis issues of the phase II data, regarding both theory and statistical issues.
- To finalise the analysis and evaluation of the 2004 data, completing the result of the experiment for phase I, and proceed with its publication.

Each of these issues is presented in detail in the following sections: analysis of 2004 data (in section 2), upgrade of the setup for phase II (in section 3), and status of the phase II operation

(section 4). Section 5 is devoted to the status of the construction of the new detection line composed of a new X-ray focussing optics and a new Micromegas detector, being built as an additional upgrade of CAST for phase II. Section 6 describes the planned schedule of the experiment for the next months and section 7 gathers the conclusions of the report.

2 Analysis of 2004 data

In 2004 CAST was running for about 6 months with almost no interruption. The homogeneity of the experiment's operation and the enhanced sensitivity of the detectors with respect to their 2003 setups provided a long high quality block of data for phase I. At the end of 2005, CAST released a first preliminary result based on the analysis of these data, and it has been already presented in several conferences in 2006. No axion signal has been detected, and therefore a 95% CL limit to the axion-photon coupling is obtained: $g_{a\gamma}(95\%) \leq 0.9 \times 10^{-10}$ GeV^{-1} for axion masses for which coherence in vacuum is preserved, i. e. $m_a < 0.02$ eV. Figure 1 shows the full exclusion plot for all values of m_a. The result is 7 times stronger than previous experimental limits and goes for the first time beyond the astrophysical limit from globular clusters as shown in the figure.

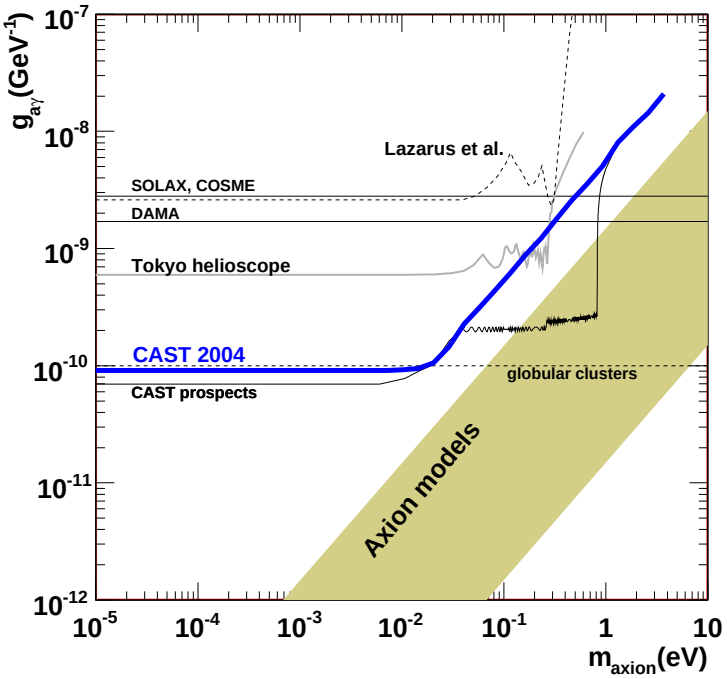

Figure 1: Exclusion limit (95% CL) from the CAST 2004 data compared with other experimental and theoretical constraints.

This analysis has recently been completed and the result is being prepared for publication. In the following we present a detailed account of each of the detector's contribution to the analysis of the 2004 data.

2.1 TPC data analysis

In 2004 the TPC was aligned with the Sun for ~ 203 hours, while the total time dedicated for background data taking was ~ 109 days. During this year the axion sensitive data are a factor 3 more abundant than in 2003 and, in the case of the background data, this factor increases to 5.

In 2003 a dependence of the TPC background on the magnet position within the experimental site was found. During 2004 a strict procedure was followed to to measure background data in all positions where the TPC tracking took place. In this way it was ensured that the contribution from the different environmental radioactivity areas to the background would follow the same pattern as in the Sun tracking spectrum.

A passive shielding, designed and built by the Particle Physics group of the Zaragoza University, was installed surrounding the TPC. The averaged data rate achieved between 1 and 10 keV was $(4.15 \pm 0.01) \times 10^{-5}$ counts/keV/s/cm^2, a reduction factor of ~ 4.3 from 2003 data. Furthermore, the data collected in the different experimental hall zones presented a high homogeneity level, proving that the shielding was able to reduce to a large extent the worrisome differences which affected the 2003 data.

The data collected in the TPC during the non-alignment periods are used to estimate the experimental background contribution to the Sun tracking spectrum. Therefore it is of great interest to identify any systematic effect which would produce a discrepancy between them.

Part of the sensitive area of the TPC is blind to the hypothetic axion signal since it does not face the magnet bores. The Sun tracking and background spectra of this area should be identical and therefore this region can be used to test all these possible systematic effects. The null hypothesis test performed on the subtracted spectrum from these two spectra yields $\chi^2/d.o.f = 28.69/29$, proving that the 2004 data are rather free from any systematic effect large enough to prevent the calculation of the axion parameters directly from the data.

Long term temporal variations related to environmental factors which can affect both the TPC background composition and nature were observed. Since they affect both Sun tracking and background data in the same way, there was no need to take them into account for the final axion analysis.

The data collected in the area of the TPC facing the magnet bores could be influenced by factors such as the magnet being energized or not, and thus the considered background is the one collected when the magnet bore status is the same as in the Sun tracking situation. This background is the one finally subtracted from the Sun tracking spectrum and for the 2004 data this subtracted spectrum was compatible, within errors, with the absence of a signal, as is confirmed by the null hypothesis test:

$$\chi^2_{\rm null}/d.o.f = 18.67/18. \tag{1}$$

The resulting data are fitted with the expected photons-coming-from-axion-conversion spectrum folded with the TPC hardware and software efficiency in order to find the best fit value for $g^4_{a\gamma}$, which was given by:

$$(g^4_{a\gamma})_{\rm min} = (1.04 \pm 1.0) \times 10^{-40}\ {\rm GeV}^{-1} \ \text{ with } \ \chi^2_{min}/d.o.f = 17.06/17 \tag{2}$$

The axion to photon coupling's upper limit has been calculated with a 95% C.L. following the Bayesian logic; the result obtained is:

$$g_{a\gamma}(95\%) \leq 1.29 \times 10^{-10}\ {\rm GeV}^{-1} \quad \text{for } \ {\rm m}_a < 0.028 \ \ {\rm eV} \tag{3}$$

Uncertainties in several theoretical parameters such as the magnetic field or the detector efficiency curve have been studied; their effect was estimated to be less than a 2% in the value of the

coupling constant given in equation 3. Furthermore, the data coming from the area in the TPC blind to any signal can be used to estimate an upper limit to this uncertainty percentage in the coupling constant value. By artificially varying the level of the background spectrum until the χ^2_{null} test on the subtracted data yields a result with a probability smaller than a 5%, this upper limit interval is found to be $\sim 10\%$. The influence of other effects such as the temporal variation mentioned before are known to be inside this range.

Figure 2 shows the TPC subtracted spectrum with the best fit (lower line) and upper limit (upper line) curves on it.

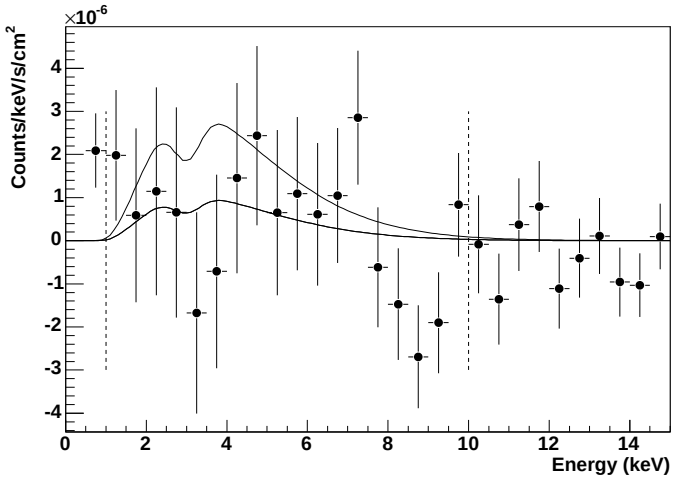

Figure 2: *Subtracted spectrum together with the best fit curve.*

2.2 Micromegas 2004 data analysis

Due to the smooth operation of CAST and the stability of the MM detector during the 2004 run, we have been able to accumulate 196h of Solar tracking data and more than 3000h of background data.

The MM hardware efficiency (fig.3) has been simulated using the GEANT4 toolkit and verified by theoretical calculations and experimental data from the prototype models that were characterized in the PANTER facilities. The dead time effects are negligible since the overall dead time is 12msec and the measured raw data rate is ≈ 1 Hz.

The offline analysis was based on a multivariate method which allowed for the identification of the signal-like events with 94% efficiency, uniform in energy, while leading to an average filtered data rate $r_b \approx 4.8 \times 10^{-5}$ events/sec/keV/cm^2 in the energy range $1 - 8.5$ keV.

In order to discover possible systematic effects in the determination of the background, various investigations were conducted, including the dependence on the position of the detector relevant to the walls and the floor of the experimental site, which act as radiation sources. The most important systematic effect was the diurnal variation of the measured rate (fig.4). This was related to the measured Rn concentration in the site which followed exactly the same pattern. The poor air recycling during the night, the increase of the humidity and the decrease of the temperature during the sunrise period contributed in the increase of the Rn concentration during the early morning hours which is the time when the MM was tracking the Sun. Therefore, we considered an effective

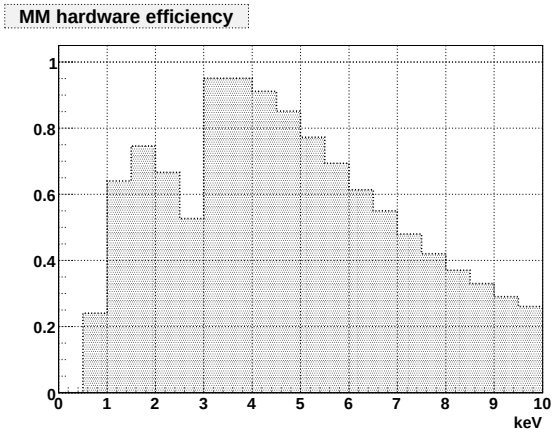

Figure 3: Simulated MM hardware efficiency where the energy binning is determined by the detector's energy resolution. The poor low energy efficiency is due to the windows between the detector and the magnet bore while for higher energies the efficiency is determined by the photoelectric absorption of the chamber's gas (95%Ar, 5% Isobutane).

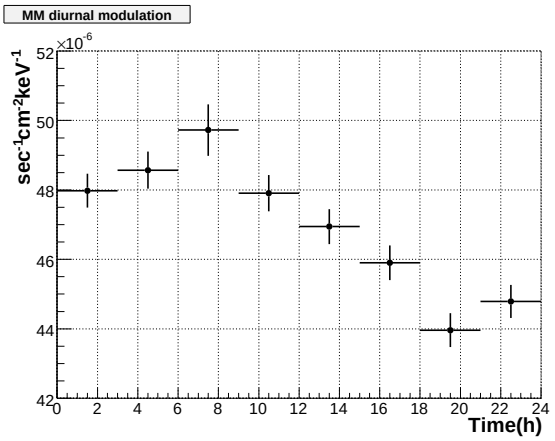

Figure 4: Diurnal modulation of the MM filtered rate.

background, measured at various time intervals around the sunrise, to be compared to the tracking data.

According to the CAST analysis strategy, the accumulated effective background spectrum, properly normalized, was subtracted from the corresponding tracking spectrum and the resulting data was fitted with the expected photon spectrum (from axion conversion) folded with the MM hardware and software efficiency. The axion-photon coupling's upper limit was then calculated following the Bayesian logic, as described in (1).

The resulting upper limits for different choices of effective backgrounds are included in tables 1 and 2; they clearly suggest that the systematic effect is only affecting the second decimal digit. Moreover minor uncertainties in software and hardware efficiencies, were simulated assuming Gaussian variations and the resulting effect is an order of magnitude weaker than the one caused by the effective background and the fitting range. Taking everything into account, we deduce the Bayesian 95%CL upper limit based on the MM data: $g_{\alpha\gamma\gamma} < 1.25 \times 10^{-10}$ GeV^{-1} with a systematic uncertainty of less than 2%.

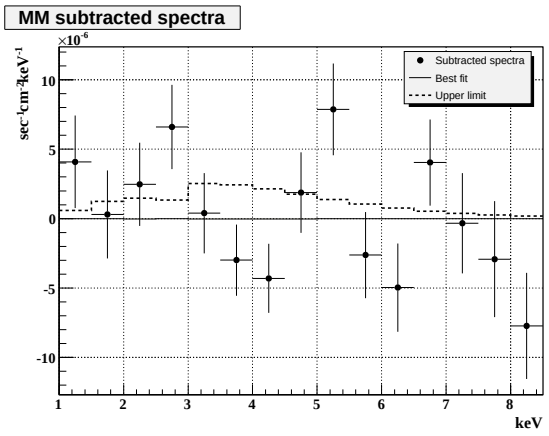

Figure 5: MM tracking spectrum after the subtraction of the effective background. The best fit and the upper limit are also visible.

Time interval	$(g_{10}^4)_{best\ fit}$	$\chi^2_{min}/d.o.f$	$\chi^2_{null}/d.o.f.$	g_{10} $(95\%\ C.L.)$
00.00-12.00	0.21 ± 0.89	$24.73/14$	$24.75/15$	1.27
01.00-11.00	-0.03 ± 0.9	$26.84/14$	$26.84/15$	1.25
02.00-10.00	-0.35 ± 0.92	$30.11/14$	$30.18/15$	1.23
03.00-09.00	-0.67 ± 0.94	$31.77/14$	$32.02/15$	1.22

Table 1: Upper limit for g_{10} from the MM data, for different choices of effective background and using the $[1, 8.5]keV$ energy range with bin size $\Delta E = 0.5$ keV.

Time interval	$(g_{10}^4)_{best\ fit}$	$\chi^2_{min}/d.o.f$	$\chi^2_{null}/d.o.f.$	g_{10} $(95\%\ C.L.)$
00.00-12.00	0.29 ± 0.9	$20.83/12$	$20.88/13$	1.28
01.00-11.00	0.06 ± 0.9	$22.26/12$	$22.26/13$	1.26
02.00-10.00	-0.24 ± 0.92	$23.93/12$	$23.97/13$	1.24
03.00-09.00	-0.55 ± 0.94	$24.54/12$	$24.71/13$	1.23

Table 2: Upper limit for g_{10} from the MM data, for different choices of effective background and using the $[1, 7.5]keV$ energy range with bin size $\Delta E = 0.5$ keV.

2.3 CCD 2004 Analysis

The analysis of the 2004 data yields no significant positive signal from axion to photon conversion over background. An image accumulated over the full observation time is shown in the left part of fig. 6. The upper limit for the axion to photon coupling could be improved to $g_{a\gamma} < 9.0 \times 10^{-11}\,\mathrm{GeV}^{-1}$ (95% CL) taking the full sensitivity of the X-ray telescope into account. In addition a toy Monte Carlo model was developed in order to test different maximum Likelihood based fitting techniques to be free of bias and to estimate systematic uncertainties.

Extensive Monte Carlo simulations with the GEANT4 simulation package have been performed, with the goal to understand the measured instrumental background of the X-ray telescope. The simulations show that natural radioactivity of detector materials, muon, and neutron induced backgrounds can be ruled out as the major contributors to the overall background. Simulations based on measurements of the environmental gamma-ray background demonstrate that this is still the dominant background component. Effects like, e.g., temporal variations of the background level during the course of the day caused by Radon could not be observed with the X-ray telescope.

The X-ray telescope data processing pipeline has been improved to be almost fully automatic, providing preliminary quick-look results of the daily solar-tracking runs within 2 hours after the run was finished. This data allows a quick verification of the performance of the detector and a check for a potential signal during phase II operation of CAST. The results of the quick-look analysis as well as the final processed data of the X-ray telescope is distributed to the collaboration via a web-interface.

3 System upgrades for phase II

3.1 Cold Windows for 0-14mbar - ^{4}He operation

After a number of successful tests with 23 μm foils, several test windows with 15 μm polypropylene (PP) foils were made before launching the production of the final windows for the ^{4}He running. The aim was to try to improve the low energy X-ray transmission for the low pressure ^{4}He running - where the gas transmission is not the dominant absorption effect. The first test was unsuccessful as the foil was glued only around the perimeter of the window and inspection under a microscope revealed imprints on the foil of the sharp edge of the strong-back wall. These imprints were caused when the foil was stretched under the 1 bar pressure difference during the test. The second and third tests were successful - the foil being glued also to the strong-back cell walls.

It was decided to launch the production using 15 μm PP and to take care that the edges of strong-back cells were not sharp. As a result, a mild electro-polishing step was included in the window flange cleaning procedure to round the edges of the cell walls. The tooling for the foil gluing was refined to minimize the glue spreading onto the foil from the strong-back. Figure 7 (left) shows the glue spreading onto the foil for window F8. The characteristic oblong surface irregularities of the PP foil at this thickness are just also visible. The strong-back cells were 5.2 mm square with wall thickness of 0.3 mm and depth of 5 mm.

Figure 7 (right) shows window F4 after the standard Cryolab test (1000 mbar He at RT, leak test, cooling to 1.9K, leak tests at 4.5 and 1.9K, removal of the He, warm-up to RT, 1000 mbar He, leak test). Characteristic wrinkles in the foil appear after the Cryolab test, these wrinkles being caused by the differential contraction of the window foil and the strong-back during cool-down which stretch the foil beyond the elastic limit.

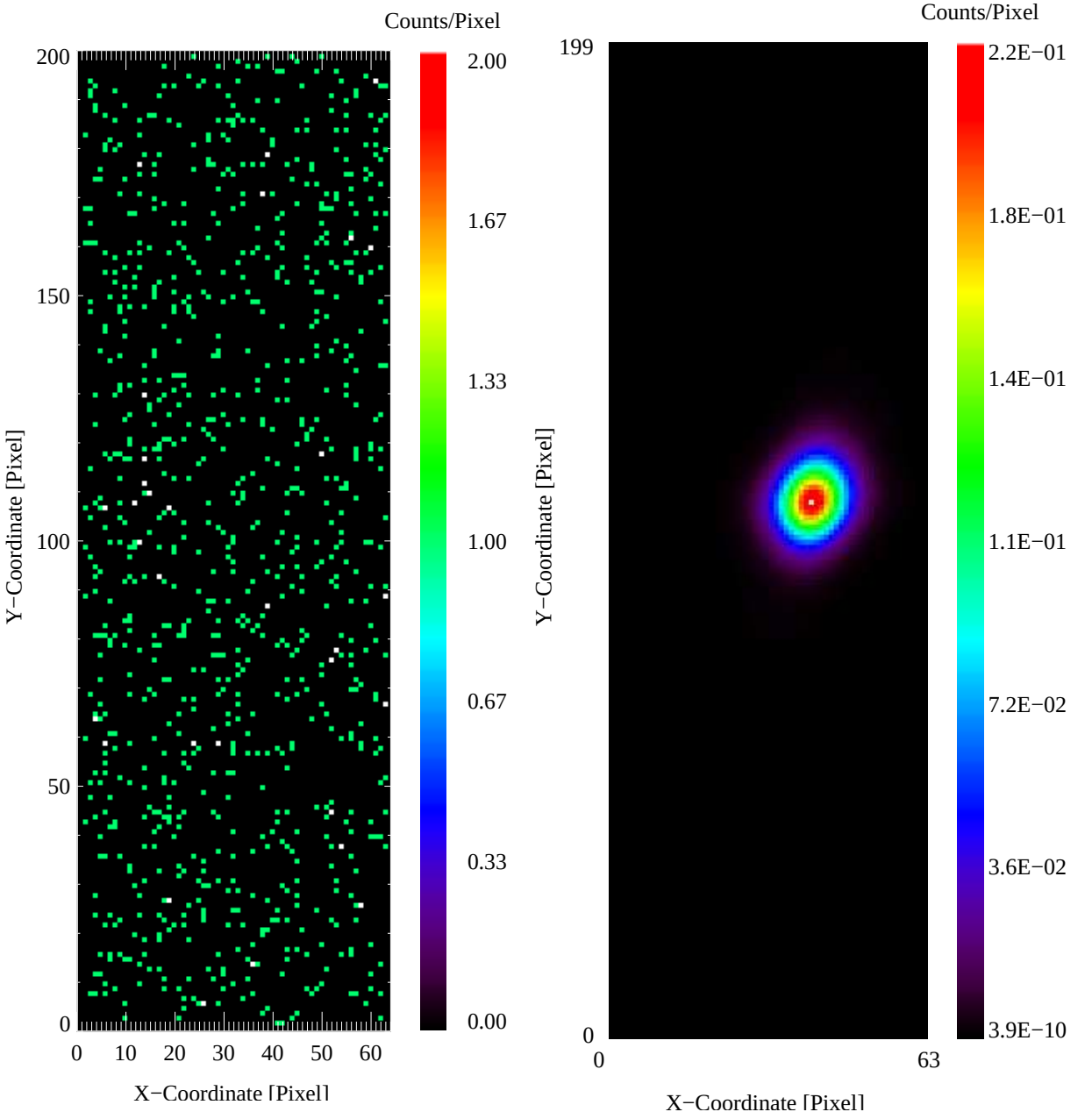

Figure 6: Left: Spatial distribution of events observed under axion sensitive conditions by the CAST X-ray telescope during the 2004 data taking period. The intensity is given in counts per pixel and is integrated over the full observation period of $t_{\text{obs}} = 707\,\text{ksec}$. Right: Expected "axion" image of the sun as it would be observed by the pn-CCD detector. To determine the axion spot on the pn-CCD, the PSF of the mirror system and the total effective area of the X-ray telescope was taken into account. The count rate integrated over the region of the spot is normalized to unity.

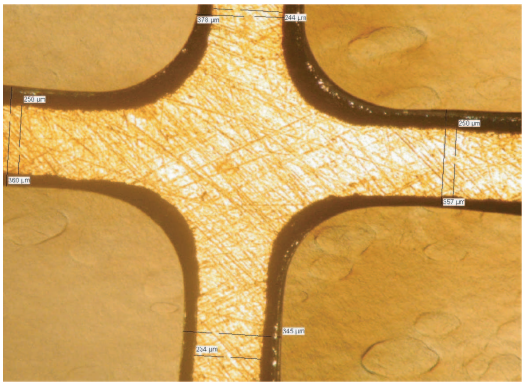

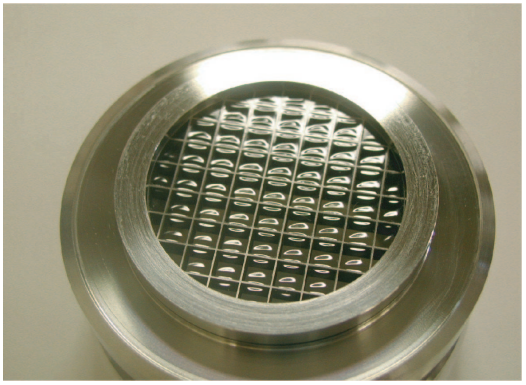

Figure 7: **Left:** Picture of window F8. **Right:** Window F4 after Cryolab test.

Figure 8 shows the calculated transmission of 15 μm PP foil not including the geometric loss from the strong-back (transmission $\sim$88%). The 15PP foil has a transmission equivalent to that of 25 μm Be, this being the target transmission for the Phase II windows (only Be foils of at least 25 microns thickness are considered pin-hole free). The 15PP window has the advantage of being constructed in-house, does not have any health safety aspects and most importantly is transparent in the visible allowing a laser alignment of the X-ray telescope.

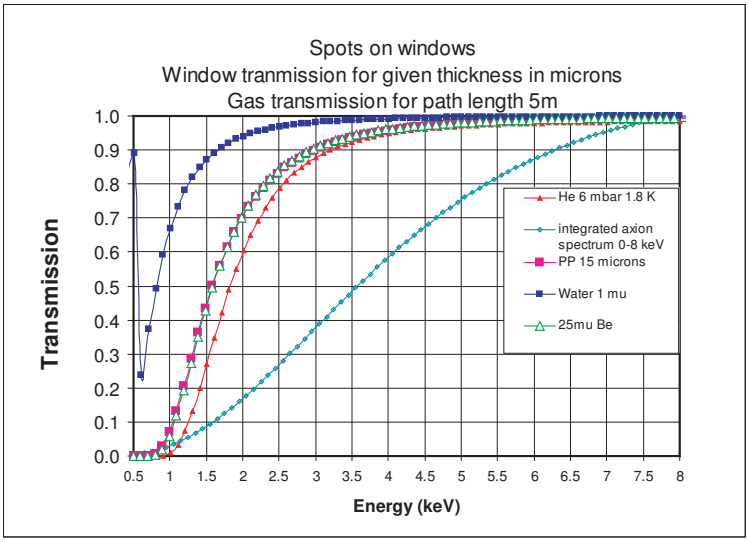

Figure 8:

A total of seven 15 μm PP windows were leak tested successfully in the Cryolab. Two windows failed the test and had to be re-glued. Five of the successful windows were also tested at the PANTER X-ray facility in MPE; all X-ray transmission measurements were identical within $\pm$2%. Indeed the measurements could not be distinguished between windows with minimal glue spreading onto the windows (50 μm) and the first two windows with $\sim$ 150 μm spread. Two typical plots are shown in figure 9.

Windows F1, F6, F7, F8 were eventually installed in the CAST experiment. One spare window, F4, has subsequently been subjected to 10 rapid (1 sec) pressurizations up to 300 mbar at a temperature $\sim$ 30K to simulate a magnet quench with 15 mbar filling of the cold bore. This successful test gave confidence that the 15 μm PP windows can withstand any quenches occurring

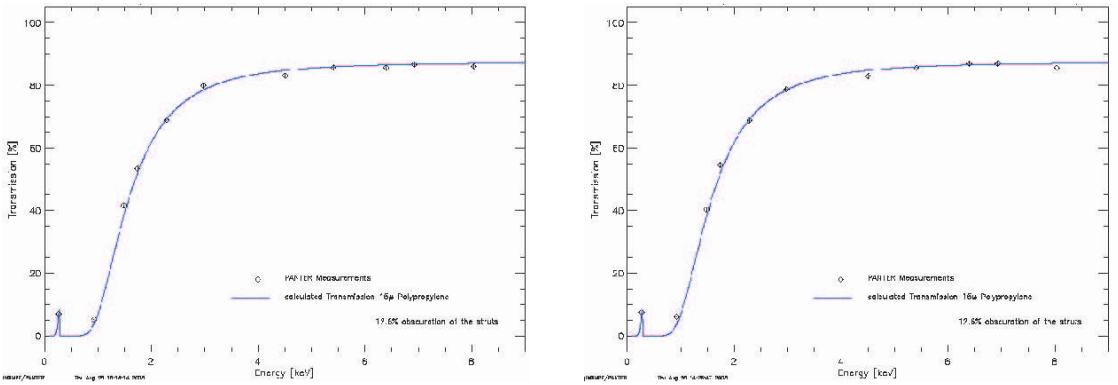

Figure 9: Transmission of cold windows F6 and F1 respectively. The diamonds show the measured transmission, the violet solid line indicates the theoretical transmission for 15 μm thick polypropylene with X-rays.

during the ^{4}He running.

One danger to these thin windows is a false manipulation of the gas and vacuum systems during installation on the magnet. After installation, the windows were leak tested at room temperature up to a maximum of 400 mbar helium in the cold bore. The helium signal measured as a function of helium pressure in the cold bore is shown in figure 10, and it is consistent with measurements in the Cryolab before installation.

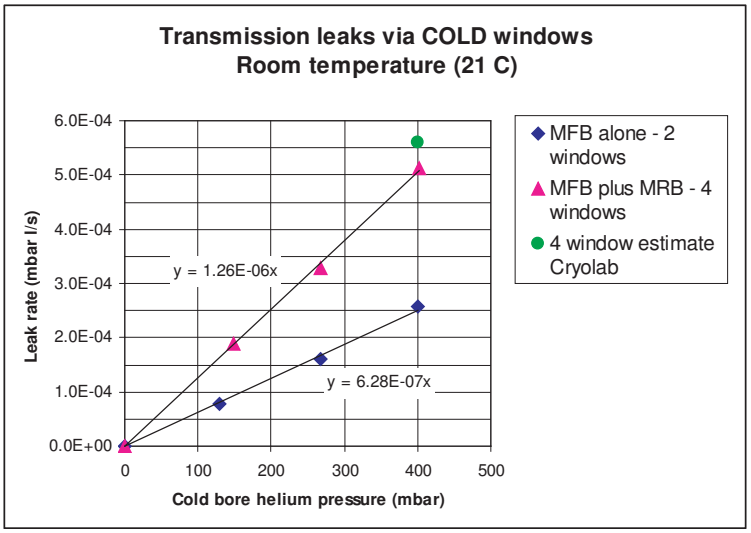

Figure 10: Window leak rates after installation in CAST.

On cooling down the magnet, the helium signal on the vacuum side of the windows was monitored by a mass spectrometer head permanently installed in the vacuum line. With 5 mbar He in the cold bore, the helium signal was $< 10^{-8}$ (mbar l s^{-1}), i.e. several orders of magnitude below the maximum operational limit for this experiment.

During the subsequent laser alignment of the CCD telescope, in October 2005, it was possible to make visual observations of the cold windows, with the magnet at 1.8K,via the view-ports of the vacuum pipe gate valves. Surprisingly, dark spots were observed on the PP foil in certain cells of the cold windows. A thorough investigation of this phenomena caused at least a 2 week delay

of the program (the TPC could not be mounted and the newly-mounted Micromegas had to be dismounted to provide the possibility to illuminate the windows).

The spots were eventually proven to be frozen gas (mainly water vapour). Recently-installed heating circuits on each of the four window flanges allowed the windows to be heated from their natural temperature ($\sim$ 50K) up to 200K. During the rise of temperature the spots disappeared. The interference phenomenon observed indicated thicknesses of typically 0.5 μm and estimates of the integrated water vapour out-gassing rates during the cool-down of the magnet were also consistent with the possibility of cryo-pumping $\sim 1\mu$m of water vapour onto the windows. The lessons of this experience are that firstly, the magnet should not be cooled down after an opening of the pipe work to moist air until an adequate pumping period has elapsed, so as to reduce significantly the out-gassing rate of the surfaces before cool-down. Secondly, the window flange heaters provide an excellent tool to bake out each of the windows independently and can be also used during cool-down of the magnet to ensure that the windows are always at a higher temperature than the surrounding pipe work and thus minimise any cryo-pumping onto the windows.

An example of the frozen gas layers 'spots' observed on the foil of certain cells on the cold window at 1.8K viewed via the TPC gate valve view-port is shown in figure 11 (left). The corresponding window 4 days later after heating the window to $\sim$ 200K and pumping is shown in figure 11 (right). The 'spots' in fact disappeared after one day of bake-out. The X-ray transmission of a 1 μm layer of water can be seen in figure 8. Even at the level of a micron thickness, the window transmission is not significantly degraded.

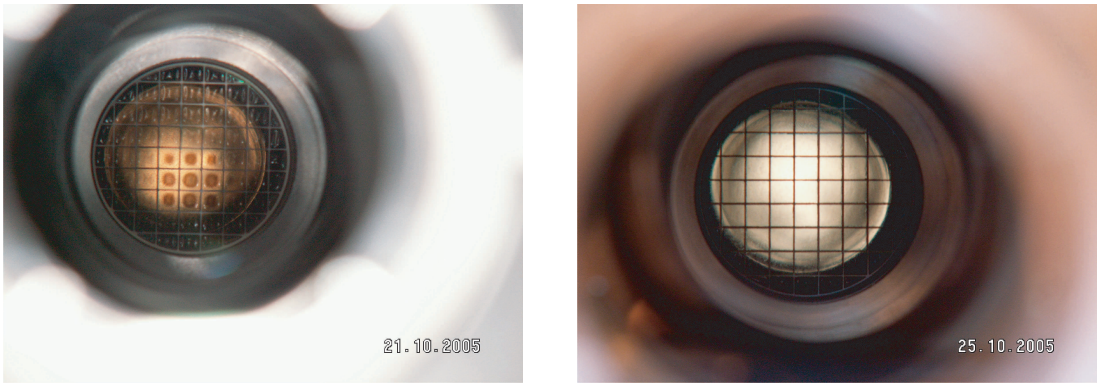

Figure 11: **Left:** Spots on cold window (temp $\sim$ 50K). **Right:** Window after heating to 200K.

3.2 Operational experience

The cold windows have now operated during 3 short data taking periods between the end of November and the present day. The windows have been thermally cycled twice, once during the end of year shutdown when the magnet was left to warm up gradually and once in February 2006 when the magnet was warmed back to room temperature for the shutdown intervention of March 2006. The windows have withstood 3 magnet quenches with helium filling the cold bore (between 3 and 4 mbar), resulting in rapid pressurisations up to 80 mbar.

On adding helium gas to the cold bore, it was observed that the temperature of the cold window flanges tends to decrease and so increases the cryo-pumping capacity of the window foils for the water vapour out-gassed from the vacuum pipe work. In addition to this water vapour from the room temperature elements of the vacuum system, there is also the out-gassing of H_2O, Ar and

CH_4 from the TPC and H_2O, Ar, iC_4H_{10} from the Micromegas. For data taking, it was decided to operate with the cold window heaters continuously powered so as to bring the windows to $\sim$120K and thus prevent Ar and limit the quantity of H_2O accumulating on the windows. In the worst case scenario, the maximum water vapour accumulated on each window is < 1 μm per month of operation. The data taking running has been organised to schedule a 3-day period for the baking-out of the windows about once per month or to initiate a bake-out whenever an interruption in data taking occurs due to unforeseen causes.

The online mass spectrometer continues to monitor the residual gas on the vacuum side of the cold windows and the total helium leak rate remains $< 10^{-8}$ mbar l s^{-1}. This rises to about 10^{-7} mbar l s-1 during bake-out due to the increased permeation of He with temperature.

3.3 Windows for 14 - 60 (120) mbar - ^{3}He running

The windows for ^{3}He running must be able to safely withstand a maximum pressure of 1.5 bar permitted by the ^{3}He safety system after a quench of the magnet with a filling of 120mbar. The present window design has already been repeatedly pressurised to 300 mbar in $\sim$1s ramp at cryogenic temperatures. Each window was also pressurised to 1000 mbar (static) between room temperature and 4.5K during the Cryolab leak test procedure. Saclay has successfully subjected a 23 μm Mylar window on the same strong-back to 5 bar (static) at room temperature. The aim is therefore to adapt the present 15 PP windows for the ^{3}He running. In the coming months, there will be a program to fabricate extra windows and test them up to progressively higher pressures whilst periodically monitoring for mechanical distortions of the strong-back, damage to the foil and measuring the leak rate. If necessary, the parameters of the strong-back will be modified until the required performance is achieved. This will first be done at room temperature then later at cryogenic temperatures. The aim is to have 4 windows plus 4 spares tested by the end January 2007, for installation in February 2007.

3.4 ^{4}He Gas system status

The ^{4}He gas system is now in operation in the CAST Phase II physics runs, which were started at the end of November 2005. The system allows confining and controlling the density of ^{4}He buffer gas in the cold bores of the magnet, and thus extending the solar axion search towards higher masses.

The fillings, in accurate density steps equivalent to pressure steps of 0.083 mbar at 1.8 K temperature, are done once per day, allowing both morning detectors (Micromegas and CCD) and evening detector (TPC) to make solar tracking with the same conditions.

Thermoacoustic oscillations (TAO) were observed in the gas system above 2 mbar pressure with an amplitude of $\sim$6% in pressure as measured at room temperature. The TAO were investigated theoretically and experimentally, and it was concluded that the phenomenon could be eliminated or at least reduced by dampers in the gas lines.

The dampers were installed close to a point where the flow is high at the fundamental mode of oscillation. Moreover, taking advantage of a planned intervention, a cold pressure transducer was installed directly in the cold bore in the MFB side. The purpose of this new pressure sensor is to verify by direct measurement inside the cold bore that no TAO occurs even in the region below the dampers.

Thus far this is true for the presently used ^{4}He buffer gas. A set of tests was made for different gas densities and cold window temperatures, showing no oscillations with amplitudes higher that

0.1% of the pressure, which is the background noise level of the sensor. This meets the specifications of CAST.

In the meantime computational fluid dynamic (CFD) simulations were started in order to investigate the effects of heat transport from hot regions to the cold bore due to convectional heat transfer. The results, still preliminary, show a small density decrease in the very ends of the magnetic length. Studies will be performed to check effects on coherent conversion of axions.

CAST is now back to the physics runs with ^{4}He gas that is expected to last until the end of the year. The upgrade to ^{3}He gas, now under design, is an ongoing task.

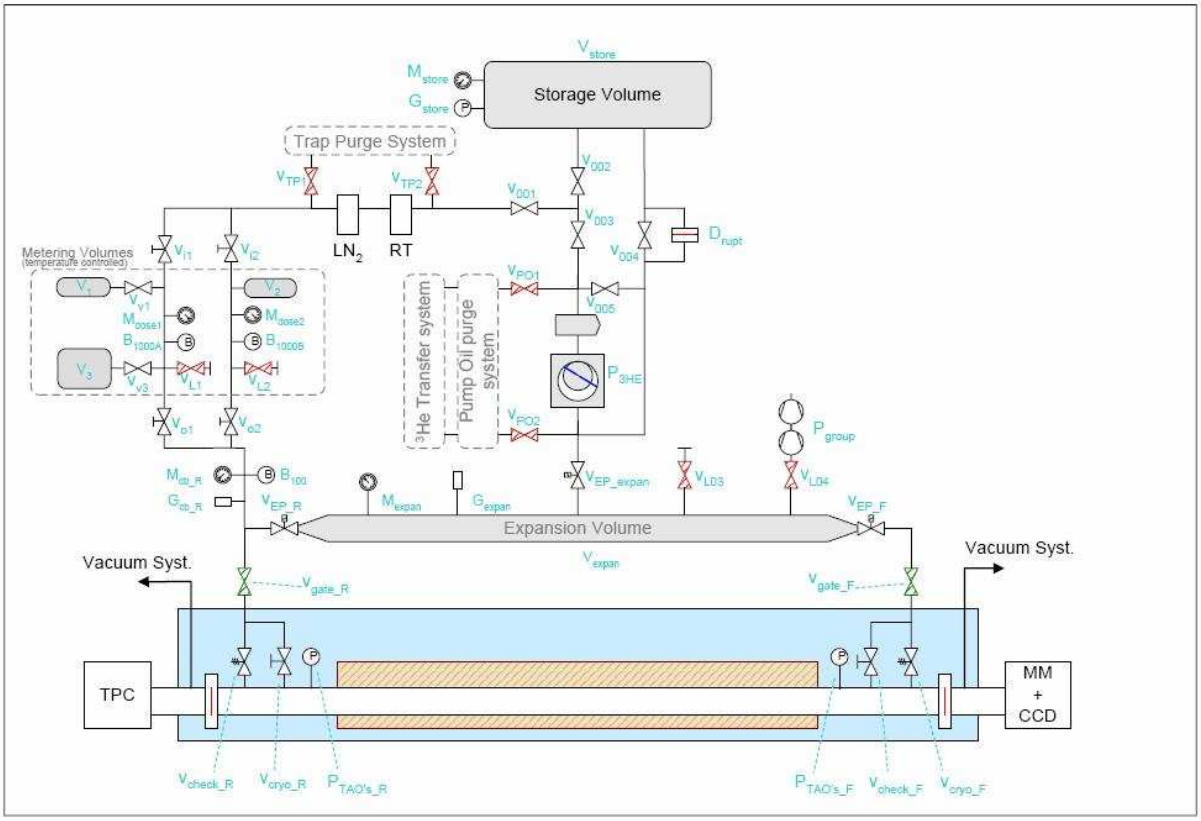

Figure 12: Scheme of the ^{3}He system.

3.5 ^{3}He Gas system design status

The main functions and requirements of the ^{3}He gas system were established. The minimal functionalities are:

- Purge of impurities in the oil of the hermetic ^{3}He pump
- Evacuation of all volumes at room temperature
- Leak testing of all volumes at room temperature
- Lossless transfer of ^{3}He from pressurized transport cylinder into the storage vessel of the gas system

- Metered and lossless transfer of ^{3}He into the magnet bores (both by stepping and by continuous ramping the density)
- Recovery without loss of ^{3}He in the event of a magnet quench
- Normal recovery of ^{3}He
- Regeneration of charcoal traps
- Transfer of ^{3}He back into the pressurized transport cylinder.
- Safety against loss of ^{3}He under all circumstances

Requirements:

- Precise metering of the amount of ^{3}He in the magnet bores (Double filling per run and possibility to make density ramping)
- Absence of thermo-acoustic oscillations
- Protection of the thin X-ray windows in the event of a quench.
- Remote data logging of the state of the gas system, without feedback
- No safety release of ^{3}He elsewhere except to the safe storage vessel.

The dimensions and specifications of the main equipment were drawn, and a Technical Design Report is under preparation, to be refereed by an external expert panel. In figure 12 are shown the main features of the system in a schematic diagram.

The total cost of the system is estimated to be about 180 kCHF.

4 Phase II operation in 2005 and 2006

CAST started data taking in phase II configuration with ^{4}He refraction gas inside the magnet bores on November 22nd 2005. After stopping for Christmas shutdown on December 14th, data taking resumed on January 19th 2006 until February 2nd. At that time stop of operation was forced by the scheduled PA8 site services maintenance, and then this shutdown was used to perform some pending interventions in the magnet. Also in this period the Sun filming and GRID measurements were performed (see following sections). Data taking could be resumed on April 29th, and it has been continued (with some occasional few days stoppages) until present. As a normal scanning protocol, the density of the ^{4}He is changed every day (after the morning shift) by an amount equivalent to 0.083 mbar pressure change at 1.8 K. This means that every detector takes data in each density step during one solar tracking. Density steps may be revisited because of operation issues of the detectors. At the time of writing this report a density equivalent to $\sim$4 mbar at 1.8 K has been reached in the scanning. In the following we give a more detailed account of the results of the last grid measurements and solar filming, as well as the specific operation issues of each of the X-ray detector during these data taking periods.

4.1 GRID measurements

As explained in past reports, CAST performs periodically the so-called GRID measurements with the help of the team of geometers at CERN. These consist in the independent measurement of the position of the magnet in a set of reference coordinates (GRID) previously defined to cover reasonably all range of movements. These measurements are intended to detect any drift in the pointing ability of the system with respect to the initial calibration values measured in 2002, the ones which are used by the tracking software to determine the real absolute direction in which the magnet is pointing at any time.

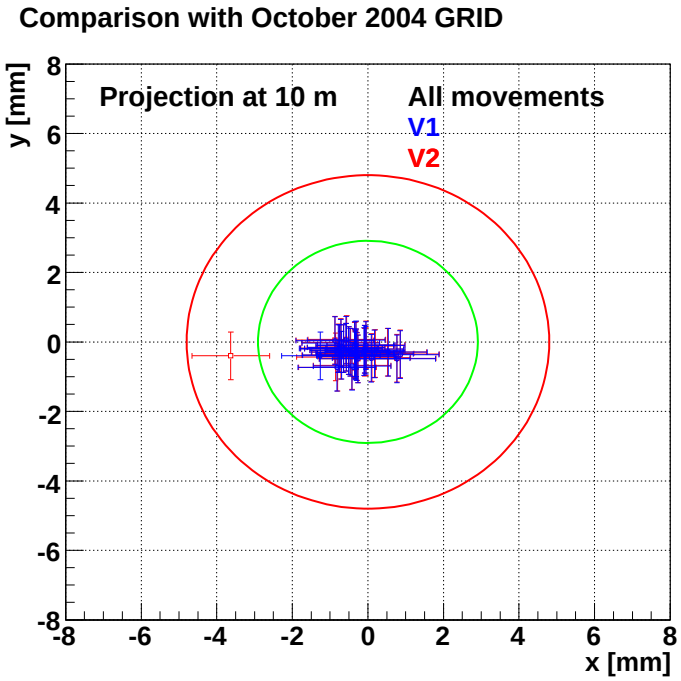

Figure 13: This plot shows the comparison between GRIDS of April 2006 and October 2004, each point corresponding to the difference of measurements at each of the GRID reference points. The green cycle is the desired precision and the red the projection of the 10% of the sun at 10 m

These measurements were performed both in October 2005 and in April 2006 and no substantial change with respect to the 2004 GRID was detected. As can be seen in figure 13, there seems to be a small shift of 0.3 mm vertical and 0.4 mm horizontal but it is much less than the desired precision. So the tracking system *is unchanged* compared to 2004.

In comparison to the reference values of the grid of 2002 (the one used for tracking) the new measurements show a shift of $\sim$1.3 mm in the vertical axis, which is due to the procedure of resetting the level value, and a shift of $\sim$1.5 mm in the horizontal axis, which is due to the extra freedom that was introduced into the system in June 2003 because of the mechanical problems with the lifting screws. This was the case for 2003 and 2004 measurements as well. However this shift is still within our acceptance.

In conclusion, the tracking system has been performing well within our requirements during last year's operation.

4.2 Solar Filming

Twice a year, it is possible to directly observe the Sun through a window in the experimental area and thus perform an optical crosscheck of the tracking system by solar filming. For this purpose, a camera is being aligned with the magnet axis and additional software is applied to consider refraction of photons in the atmosphere.

The solar filming has been repeatedly performed during the past. Thus for the 2003 and 2004 data taking phase it was confirmed that the magnet was pointing to the Sun while taking data with the accuracy required. Until March 2005, a webcam in combination with a small telescope was used to film the Sun. In order to improve the resolution and the alignment, the system was enhanced to provide a precision which matches the desired accuracy of the solar tracking (0.02°). Therefore, the new filming system consisted of an ST-7 CCD camera and better optics with 200 mm focal length. Furthermore, the concept used to align the filming setup with the optical axis of the magnet was changed. Thus a higher accuracy of the measurements and a better quality of the images was achieved.

Already first tests in spring 2005 showed that the CAST magnet was pointing to the center of the Sun with an improved precision of the optical crosscheck, namely O(0.03°). A further enhanced setup was used in fall 2005. Not only was it made to be more rigid and thus damping the vibrations but also to be more flexible and hence easier to align with the magnet axis. With this latest setup a precision of 0.02° could be achieved at best and thus the accuracy of the tracking system could be reached. Within this precision, the magnet is pointing to the solar core from which most axions are expected to emerge. For March 2006 the analysis of the solar filming leads to a similar result with an even slightly improved accuracy of 0.015°; hence within the desired precision the CAST magnet is pointing to the center of the Sun.

4.3 TPC operation

The Time Projection Chamber (TPC) of the CAST experiment has been operating continuously from the beginning of CAST second phase. The TPC is a wire chamber using Ar-CH_4 gases, which makes use of the ALICE Front-end Digital Card prototype electronics.

4.3.1 TPC setup upgrades

The development of two new differential windows made of 4 μm polypropylene has improved the leak rate towards the magnet achieved for the first phase of CAST. The pumping system decreases the leak rate of the detector by a factor $\sim$700. The second phase setup improves a factor 5 for Ar and a factor 35 for CH_4 compared to the best leak rates measured in 2004. This improvement has been important in CAST second phase, due to the existence of cold windows keeping the He gas needed to restore the coherence of the axion-photon conversion. Higher leak rates would provoke atom layer deposition on the cold windows inside the magnet and therefore reduce the efficiency of the experiment.

A new quadrupolar power supply has been adapted to the preamplifiers of the TPC. The new device, a TENMA 72-6905 has low ripple and noise (< 2 mV rms). The power supply is equipped with an overload and reverse polarity protection allowing the TPC DAQ to decrease the noise levels of 2004 and makes the operation of the preamplifiers safer avoiding the lose of channels due to voltage spikes.

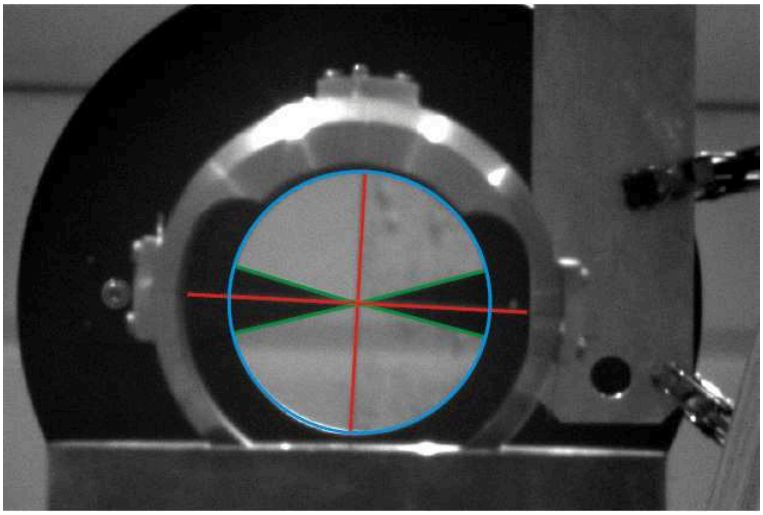

Figure 14: Alignment picture taken on 28.09.2005. At 5 m distance of the camera cross-hairs inside a sphere with the specifications of a Taylor-Hobson sphere are placed to mark the optical axis. At 7 m from the ST-7, a pointer indicates the same axis. As can be seen the crossing point of the wires and the tips of the pointers are in line and thus the filming setup is well-aligned.

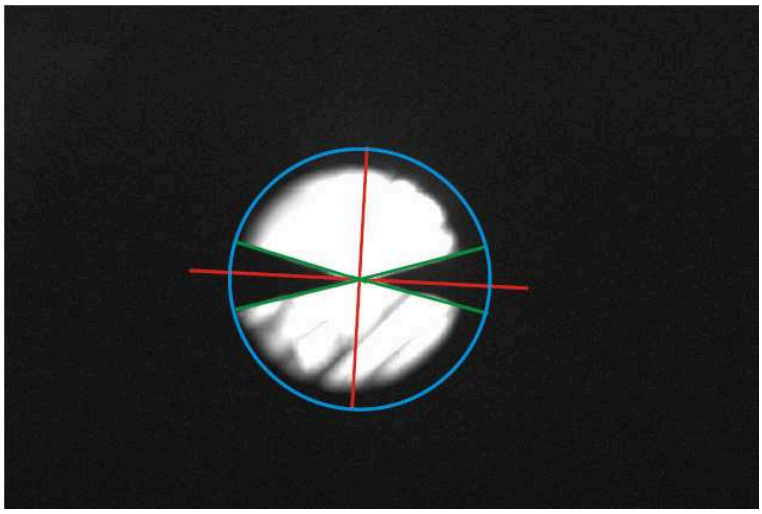

Figure 15: Superimposition of about 75 pictures taken during filming on 28th September 2005. For reference the crosshairs, the pointers and the circle, within which a full view of the Sun is possible (i.e. no disturbances due to disk of pointers or sphere occur), are added in the picture.

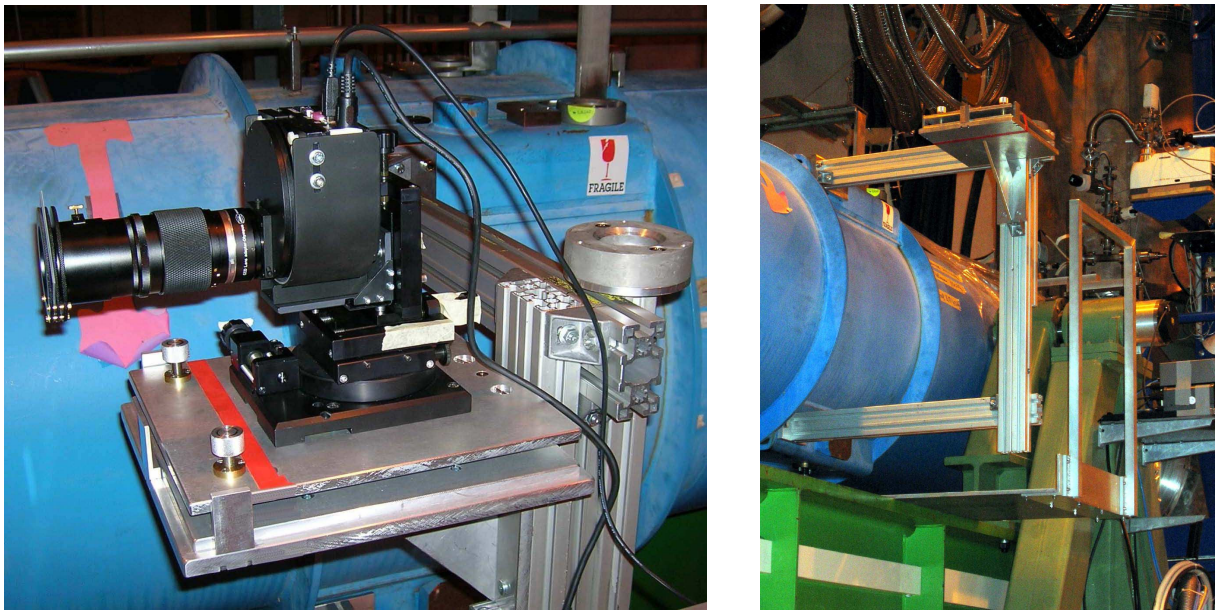

Figure 16: **Left:** The filming system is mounted on a tiltable platform on the console fixed to the Rexroth Profiles. It simplifies the vertical alignment of the optics. A support allowing movements of the camera in all spatial directions holds the ST-7 and is screwed to the inclinable platform. **Right:** The new side arm for the filming system constructed by using Rexroth Modular Profile Systems is fixed to the magnet. A console is attached to the vertical profile. It can be moved up and down to bring it into any desired position. Thus a rough adjustment of the filming system can be performed.

The passive shield installed around the TPC was the same one already used in 2004. The final setup of the shield is composed of 225 mm of polyethylene, 1 mm of cadmium, 25 mm of lead and 5 mm thick copper box which encloses the TPC detector. The flushing of nitrogen gas inside the copper box creates an over pressure which helps, together with a plastic bag which seals the whole structure, to decrease radon contamination.

Fig. 17 shows the comparison between the 2004 and 2006 background levels for the TPC in the CAST experiment.

X-ray absorption in the 15PP cold windows in front of the TPC (see section 3.1) reduces the TPC detection efficiency and must be included in the overall efficiency curve of the detector. Figure 18 shows the evolution of the efficiency curves of the TPC between Phase I and Phase II

4.3.2 TPC data taking

The TPC detector has been operating in the second phase of the CAST experiment since November 2005. The first set of density steps were taken from November 22nd until December 14th. During this time the TPC had noise problems with the old power supplies of the preamplifiers and some of them died due to spikes of the low voltage. This problem was solved for the next period of data taking that took place from January 19th of 2006 until February 2nd of 2006.

From April 29th until May 14th the third data taking of CAST second phase took place and an improvement of the shielding against Radon lowered the level of the background spectra.

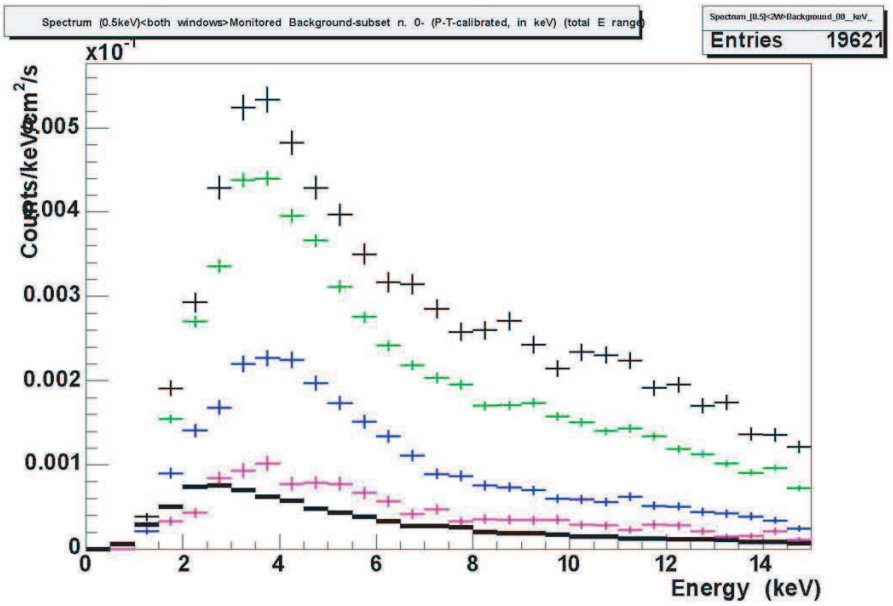

Figure 17: Comparison between the different levels of background that the TPC has for each of the different steps of the shielding installation. The black line shows the 2005 background spectrum of the TPC without shielding; the green line shows how the background changes as soon as the first pieces of shielding are installed; the blue line shows the background obtained with the copper box and the front part of the shielding and the pink line shows the background spectrum once the shielding is finished. The difference between pink line and the thick black line is due to the active shielding against Radon by flushing with Nitrogen gas at 250 l/hour the volume of the TPC.

4.4 Micromegas operation

The Micromegas detector was installed for operation in CAST second phase in identical setup as in 2004, known as V4. The only relevant difference was the material of the drift strongback, now being of aluminium while before it was stainless steel. This change was made to reduce the contribution of the iron fluorescence to the experimental background in the region of interest.

Data was taken continuously during the first 2 sets of runs in November-December 2005 and January-February 2006. The operation conditions were good and very stable (gain, resolution, pulse and event characteristics, software cuts efficiency,...). The background level was good (about 3.5×10^{-5} c/keV/cm^2/s) and its shape is understood, as can be seen in figure 19.

During the installation of the detector for the 3rd data taking period (which started the 29th April), an incident forced the replacement of the prototype by a newer one, known as V5, never before used in CAST. Although identical in design, V5 has an improved feature with respect to V4: the amplification mesh has been coated with gold, for the purpose of stopping the 8 keV photons coming from copper fluorescence, which, as seen in fig. 19, dominates the detector background. In spite of this unforeseen replacement of the Micromegas detector, which introduced the risk of possible unknown effects of the new prototype, V5 proved to operate reliably. The only drawback with respect to V4 was the presence of a few dispersed dead strips, which caused the strip signal of the events to be slightly degraded with respect to V4, and in consequence the software cuts slightly less powerful in rejecting background. On the other hand, however, the expected effect of the gold coating was very soon evident, and the copper peak at 8 keV –always present in past spectra– has almost disappeared as shown in figure 20. In summary, the V5 data taking conditions and their

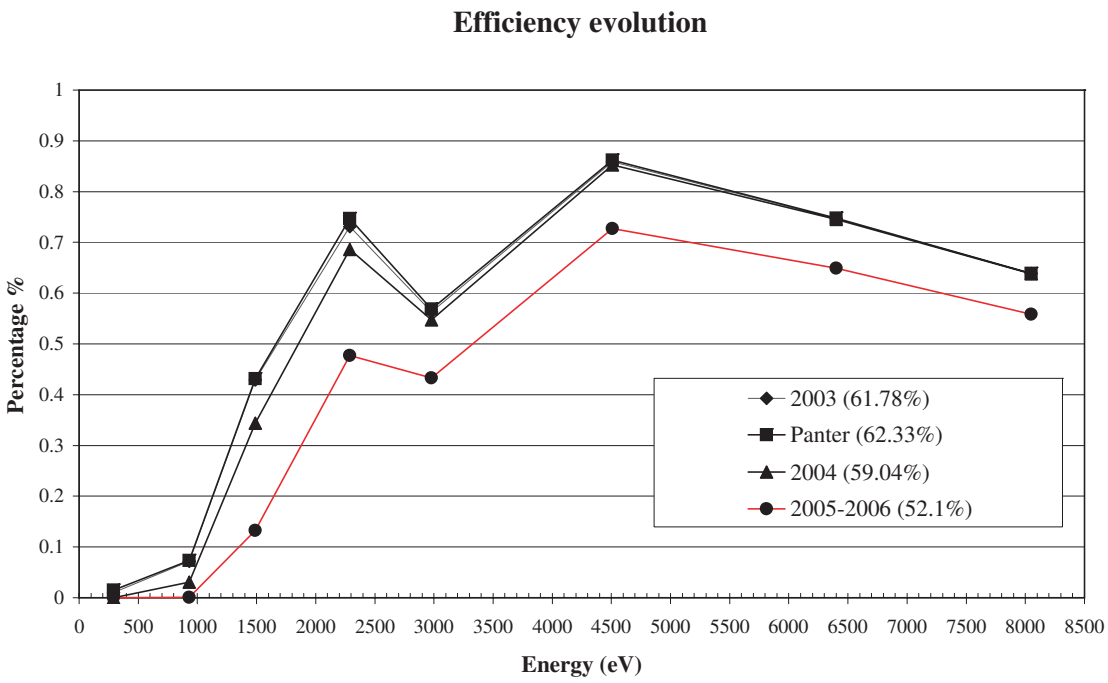

Figure 18: Efficiency curves for the TPC of the CAST experiment for First and Second Phase.

data quality are, at the least, equivalent to the V4.

Since its installation, the V5 detector was operational in all density steps scanned by CAST, and it is presently running. V5 data shows also a high quality (with the only issue of the missing strips) and very good stability. It is foreseen that it will remain in operation in CAST until the new detection line will be installed (see section 5), which is scheduled for September 2006.

4.5 pn-CCD and X-ray telescope operation

The pn-CCD detector was operated during the 2005/06 data taking period in the same configuration as during the 2005 data taking phase. Both, the detector performance and the background count rate was stable at a level of $(9.61 \pm 0.37) \times 10^{-5}$ counts cm^{-2}sec^{-1}keV^{-1}, which corresponds to (0.19 ± 0.01) counts per tracking run. Further modifications to the system were not necessary since the telescope reached it's maximum sensitivity. Regular measurements with an X-ray source were performed to verify the stability of the alignment of the system over the data taking period based on reference measurements made in 2004.

5 New detector line with 2nd telescope

The design of the new Micromegas line consisting on a new x-ray focussing optics, a new detector and an adapted shielding has been finalised. A view of the final design can be seen in figure 21. The X-ray optics can increase sensitivity to the axion coupling constant by reducing the spot on the detector from the width of the magnet bore to a few mm, leading to a significant reduction in the background. The new smaller detector will profit from a higher efficiency due to the use of a heavier gas (Xe-based mixture). The shielding will protect the Micromegas detector from a

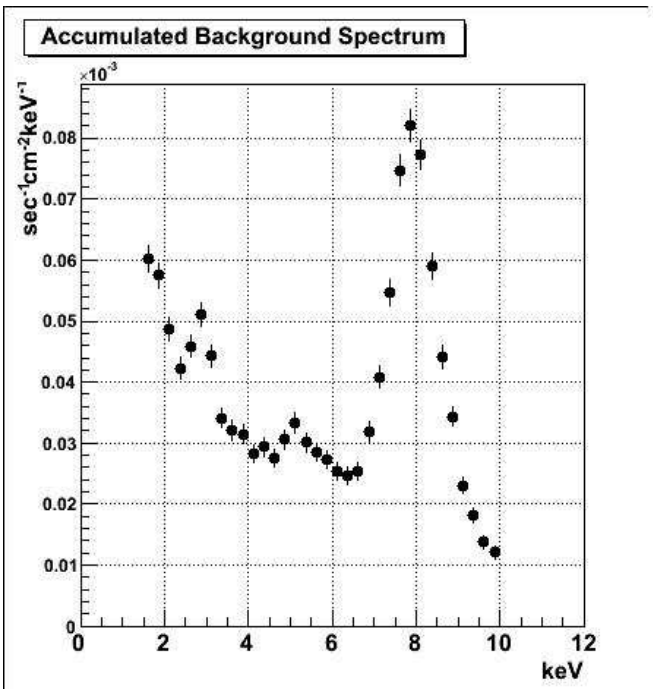

Figure 19: Background spectrum accumulated by V4 detector during the two first sets of runs of Phase II, i. e., from November 2005 until Febrary 2006. It is dominated by the copper fluorescence peak at 8 keV. Also visible are the copper escape peak at 5 keV, the Argon fluorescence at 3 keV and, maybe, part of the aluminium peak at the lowest part of the spectrum.

fraction of the cosmic rays and natural radioactivity. The TPC experience shows that the reduction of the level of background will be about a factor of 4. The shielding will consist on 0.5 cm of copper and 2.5 cm of lead in a flux of N_2 gas. The gas tightness will be obtained by a plexiglas enclosure. On the plexiglas, blocks of polyethylene of 20 cm will cover the whole enclosure as can be seen in figure 21.

5.1 New Micromegas detector: first tests

A first prototype of the detector has been mounted and tested. As a Xenon gas mixture will be used, a more sophisticated gas system has been designed for the operation of the detector in a semi-sealed mode by using a calibrated leak that will maintain the gas conditions constant. Tests on the gain and stability in the semi-sealed mode have been successful.

The new mechanical assembly has resulted in a better energy resolution (better than 12% (FWHM) compared to 20%).

Presently the final detector is being mounted and tested. The rest of the line, platform and services (gas, vacuum, calibration) are being mounted in order to be ready for the calibration test at the PANTER X-ray facility scheduled end of August where the detector as well as the X-ray optics will be characterised.

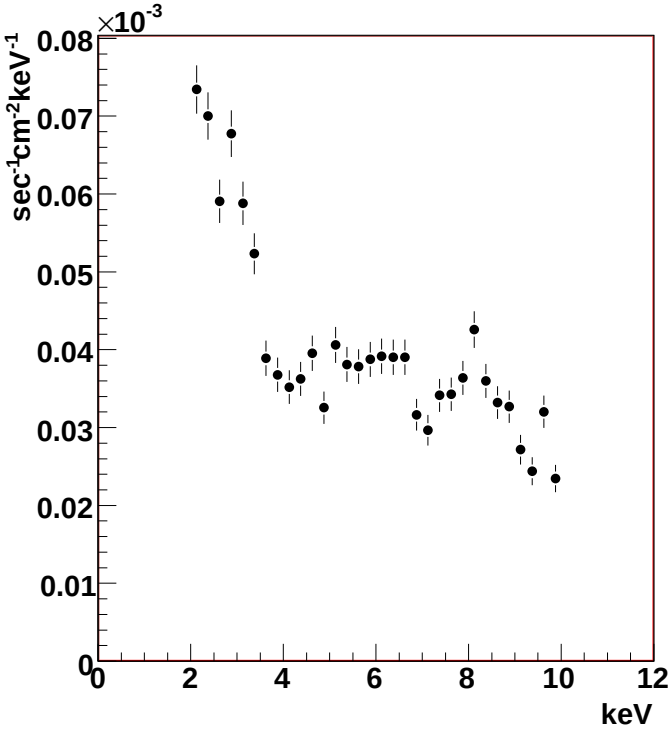

Figure 20: Background spectrum of the V5 detector

5.2 Second X-ray Optic

5.2.1 Overview

The use of a X-ray optic focuses the putative X-ray signal from the width of the magnet bore (42.5 mm) to a very small spot just a few mm in diameter. This scheme reduces the required active detector area by at least a factor of 100, leading to a corresponding decrease in background, and thus, higher sensitivity. Due to the successful implementation of the *ABRIXAS* flight telescope on one of the four magnet bores, it was decided to employ a second X-ray optic to work with a new Micromegas detector.

A detailed Monte Carlo study was performed to optimize the optical parameters specifically for the CAST experiment. Rather than use a traditional Wolter telescope design, we have selected a novel collimator design suited to the physical constraints of the experimental hall and the existing telescope + CCD line. Table 3 lists the basic properties of the new optic. For reference, the spot size and throughput are nearly identical to that of the ABRIXAS telescope. Additional details can be found in the 2005 SPSC report (`CERN-SPSC-2005-022`).

5.2.2 Fabrication Process

The collaboration endorsed the plan to install a new optic on the Micromegas beamline in Spring 2005, and work on the construction began in Summer 2005. In the most general terms, the fabrication of the optic can be divided into four phases. First, each of the fourteen polycarbonate substrates must be produced. Next, each of these substrates must be coated with a thin film of iridium. In the third step, the coated substrates must be mounted into a structure that maintains the

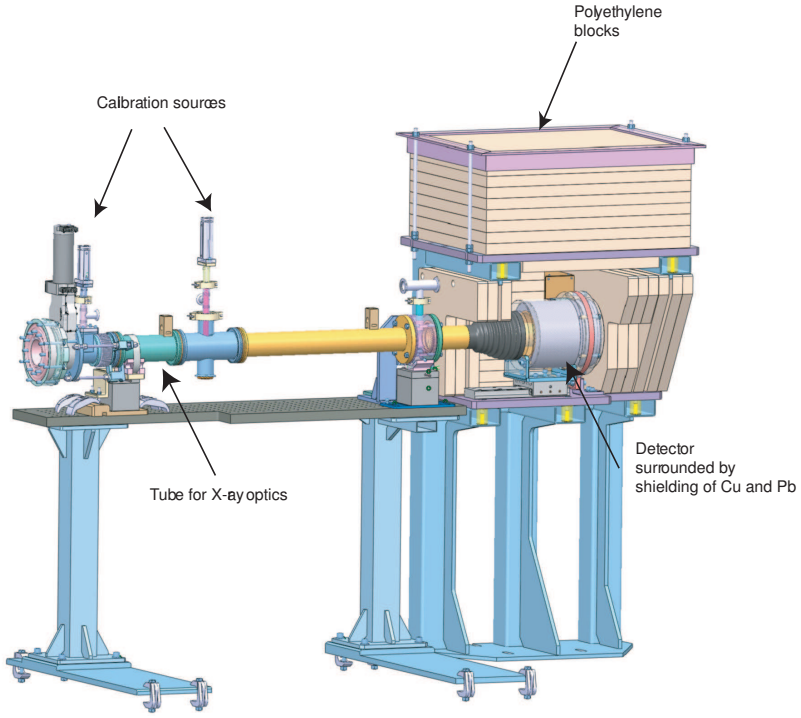

Figure 21: The new Micromegas line on its platform. The emplacement of the X-ray optics is shown. The detector is positioned at the focal point of the collimator (1.3 m away), surrounded by its shielding. Two calibration sources have been foreseen in order to assure the alignment of the line as well as the calibration of the detector.

Nested Shells	14
Length	117.5 mm
Focal Length	1.3 m
Coating Material	Iridium
Coating Thickness	300$\pm$50 Å
Throughput	36%
Spot-size	$<$3 mm (diameter)

Table 3: Properties of the CAST X-ray Collimator

relative alignment of all of the shells such that the individual mirrors act as one coherent optical element. Finally, the optic is mounted inside a structure that itself attached to the inside of a vacuum vessel by a series of flexures that allows precise alignment of the optical axis to the magnet bore.

Unfortunately, depositing a uniform, smooth layer of iridium on the interior of the integral cones with large aspect ratios (diameters as small as 18 mm) proved more challenging than originally indicated from preliminary investigations. An intensive Research and Development program between LLNL and AxynTec, a commercial company located in Germany, ultimately achieved the required performance, largely in part due to the exhaustive metrology performed at LLNL. Examples of these measurements include SEM (figure 22 [*left*]) that verified the thickness of the coating and AFM (figure 22 [*right*])that verified the micro-roughness.

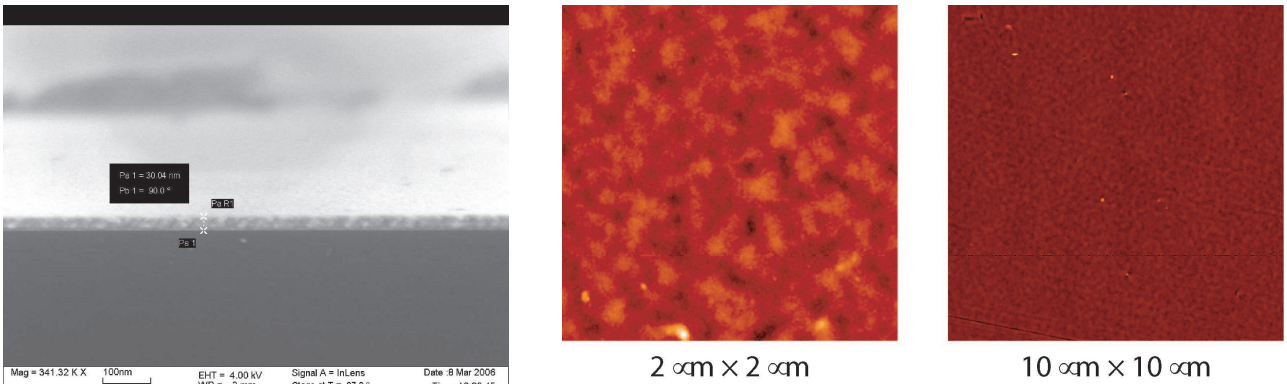

Figure 22: **Left:** SEM measurement of a Si witness coated with iridium during a qualifaction deposition process. The measured thickness of 300 Å falls exactly within the desired range. **Right:** AFM measurements performed on a piece of polycarbonate substrate coated with 300 Å of iridium. Analysis of these AFM scans indicate a micro-roughness in the range $\sigma \approx 10 - 15$ Å.

5.2.3 Schedule

The first complement of fourteen iridium-coated cones (figure 23 [*left*] is a photograph of 11 of these cones) was received at LLNL in late June. Assembly into the final optic (figure 23 [*right*] shows an engineering drawing of this nested optic) will be completed by mid-July, 2006. The vacuum vessel and additional mounting hardware have already been completed, and installation of the optic into its vacuum assembly will be completed by early August, 2006.

Detailed calibration of the optic, including its effective area and point spread function, will be performed at the MPE PANTER facility in late August, 2006. The three week experimental campaign will include testing of the optic by itself, testing of the new Micromegas detector, and testing of the optic and Micromegas working as one integrated unit as it will deployed on the CAST apparatus.

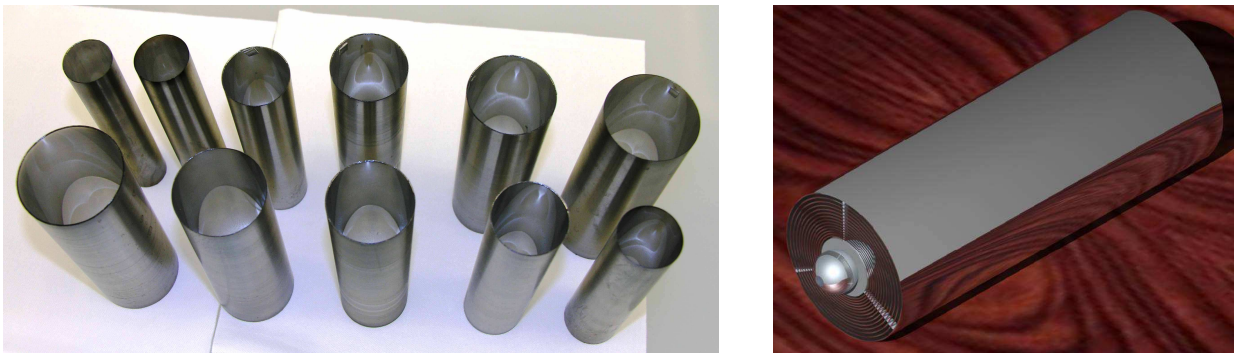

Figure 23: **Left:** Photograph of 11 iridium coated polycarbonate substrates, prior to integration into the optic assembly. **Right:** Engineering drawing of the completed nested optic.

6 General schedule for next months

The CAST schedule for 2006 is to complete the data taking with ^{4}He, approaching as near as possible to the limiting pressure of 14 mbar (1.8K). Taking into account window bake-outs, quenches

and other stoppages, this requires $\sim$150 days or 5 months at one density step (typically equivalent to 0.083 mbar step in pressure) per detector per solar tracking and will require running until the end of year shutdown.

Operation with at least two pressure steps per solar tracking is essential for the ^{3}He running in 2007 in view of the many steps needed for the scan to approach the density equivalent to 50 mbar pressure. The optimal way to cover the equivalent of a double pressure step per solar tracking is under study; being either a rapid, discrete step in the middle of the tracking or a continuous ramp throughout the tracking. The former method can be tested in CAST with the existing gas system but would require the duplication of some components of the gas metering system before being fully operational for data taking. The latter method will be tested in a prototype pressure ramping system in the Cryolab later in the year and may be available to be tested in CAST near the end of the year.

The new Micromegas-line (MM-line) is expected to be available for installation towards the end of September 2006 and the installation, alignment (MM-line and CCD telescope) and commissioning is estimated to take about 5 weeks (the magnet will remain cold). At this time, the collaboration will decide on the optimal moment to install the MM-line. In mid-September 2006 the helium density should have reached the equivalent to $\sim$9 mbar at 1.8 K or m_a $\sim$0.31 eV and allowing for the MM-line installation and continuing with single step operation until the end of year a maximum density equivalent to a pressure of $\sim$12 mbar at 1.8K, or m_a $\sim$0.37 eV can be reached.

The installation of the ^{3}He system is now foreseen for the first half of 2007. In parallel with the data taking in the second half of 2006, the ^{3}He system road map is foreseen as follows:

End July 2006

- Complete the Technical Design Report
- Submit to CERN cryo-safety committee. Submit to an external referee(s)
- Launch any outstanding calls for tender
- Conceptual design study of integration of components inside cryostat
- First discussion with Central workshop the intervention at end of 2006
- Final cost estimates

August 2006

- Complete MOU to allow spending

September 2006

- Technical Design Review
- Green light to start ordering system

October 2006

- Start execution drawings for integration of components inside cryostat

November-December 2006

- Preparation of pipe-work, volumes and support structures

Mid-December 2006

- Warm magnet to room temperature

January - April 2007

- Open magnet
- Installation of 3He system inside and on the exterior of cryostat
- ^{3}He cold windows must be ready for installation (end February)
- RT commissioning tests with ^{4}He

April- May 2007

- Close magnet and cool down
- Commission systems in readiness for data taking

The data taking starting in June 2007 with double step operation should approach 45 mbar ($m_a \sim 0.71$ eV) by the end of 2007. The ^{3}He system will have a pressure reach up to 120 mbar ($m_a \sim 1.16$ eV) which could be attained by two additional years running. To fully exploit this potential, CAST will request operation time for 2008 and maybe part of 2009.

7 Conclusions

The present status of CAST has been described. The collaboration has recently finished the analysis of 2004 data and is preparing the corresponding publication. Work on the upgrade of the experiment, specially concerning the cold windows and the ^{4}He gas system, has been successfully accomplished to start phase II with ^{4}He. The physics runs with this setup, which should allow CAST to scan axion masses up to $\sim$0.40 eV, started last November and should last until the end of this year. In parallel, considerable progress has been made on the second step of the upgrade, which contemplates the operation with ^{3}He in the magnet pipes. The road map for the construction and installation of the ^{3}He setup has been presented. This new setup will extend the sensitivity of CAST up to $\sim$1.16 eV in further density steps that will start by mid of next year.

References

[1] K. Zioutas *et al.* [CAST Collaboration] Phys. Rev. Lett. **94** (2005) 121301 [arXiv:hep-ex/0411033].